Is the dewatering of Palm Oil Mill Effluent (POME) feasible? Effect of temperature on POME's rheological properties and compressive behavior

Sabeeha.N.B.A.Khadaroo [a], Paul Grassia[b], Darwin Gouwanda[a], Phaik Eong Poh[a*]

[a] Chemical Engineering Discipline, School of Engineering, Monash University Malaysia, Jalan Lagoon Selatan,47500, Bandar Sunway, Selangor, Malaysia

[b] Department of Chemical and Process Engineering, University of Strathclyde, James Weir Building, 75 Montrose St, G1 1XJ, UK

*Corresponding Author Email: poh.phaik.eong@monash.edu Tel: + 603 55146272 Fax: + 603 55146207

Abstract

The current treatment process of Palm Oil Mill Effluent (POME) has been a cause of concern over recent years as POME is known to cause greenhouse gas emission as well as water pollution. An alternative for POME treatment process optimization is to eliminate the conventional cooling ponds and introduce a dewatering device such as a thickener. The thickener will assist in the solid-liquid separation, removal of microbes and other impurities from the wastewater. The latter will contribute to making the anaerobic digesters used to treat POME more efficient by allowing a means of control on the digesters' load. However, to be able to design and predict the performance of the thickener unit; essential rheological properties of the suspension have to be determined. The rheological characteristics and the compressive behavior of POME have not been studied previously nor has the implementation of such a dewatering device in the POME treatment process. This paper attempts to bridge the gap on the rheological characteristics, the compressive behavior and the effect of temperature on the rheological properties of POME through batch settling and batch filtration experiments. Data such as the compressive yield stress, the hindered settling function, and the diffusivity function for POME have been extracted and evaluated.

Keywords: Palm Oil Mill Effluent, Batch Settling, Batch Filtration, Compressive Yield Stress, Hindered Settling Function, Diffusivity Function

Table of Contents

1. Introduction

Every ton of Crude Palm Oil (CPO) produced generates approximately 3.05 m^3 of Palm Oil Mill Effluent (POME) (Hassan et al., 2005). POME is considered as one of the most challenging waste products to dispose of in the palm oil industry due to its high organic content. Therefore, an effective technique for disposal is of paramount importance. Nevertheless, when treated efficiently, POME can provide useful products such as biogas and A grade biosolids that can be used as fertilizers. Furthermore, the Malaysian government has recognized the prospect of using POME as a renewable energy resource (Choong et al., 2018). Malaysia's National Key Economic Area for Palm Oil industries have 2 specific Entry Point Projects (EPP) related to palm oil mills, EPP4 which aims to improve the oil extraction rate and EPP5 which entails developing biogas facilities for palm oil mills; however, the issue with EPP4 is that some mills incur high oil loss through waste streams. It is thus essential to implement sustainable practices in the palm oil industry to be able to extract the residual oil in the waste stream and generate as well as capture biogas as it is a potent source of renewable energy. There are still more than 85% of palm oil mills in Malaysia that continue to use not biogas facilities but rather the ponding system owing to the low cost associated with the latter for the treatment of POME. In addition to the drawback of the excessive use of land for the ponding system, the emission of greenhouse gases (GHGs) to the atmosphere is a consequential environmental burden being encountered with the current treatment process.

Every tonne of POME treated by the ponding system has the potential of generating about 12.4 kg of methane gas (Choong et al., 2018). Another significant concern is that POME can cause water pollution when discharged in watercourses due to the presence of organic matter which can decompose easily. This, in turn, results in a high content of Chemical Oxygen Demand (COD) and Biological Oxygen Demand (BOD) of 51,000 mg/L and 25,000 mg/L respectively

(Choong et al., 2018; Iskandar et al. 2018). High COD and BOD effluent content contribute to the oxygen content in the water to be curtailed which gradually hinders the growth of the aquatic life and in the long term may cause their extinction (Iskandar et al., 2018). The treatment of POME is, therefore, a high priority concern which needs to be addressed promptly since the global demand for palm oil is predicted to increase unceasingly in the years to come. (Tabassum et al., 2015).

The impediment with the current treatment process is that POME discharged at 80-90℃ is sent to the cooling ponds where the residual oil is removed from the surface in addition to allowing the temperature to drop so as to achieve an adequate temperature for mesophilic anaerobic digestion. This process of oil extraction from the cooling ponds is highly ineffective, and there is considerable heat loss to the atmosphere. The introduction of a thickener will however allow the oil, liquid and solid portions of POME to be separated. The residual oil can be scraped off and material that easily settles out will be removed, resulting in a homogeneous effluent and a sludge discharge that can be sent for further treatment. The appropriate discharge sludge to liquid ratio will then be sent to the anaerobic digester at a higher temperature such that thermophilic anaerobic digestion can take place (Appels et al., 2008). This modification in the process demands a measure of control on the anaerobic digester's load.

As a consequence of this alteration, the anaerobic digestion process is expected to be more stable, and the amount of biogas produced should increase. The thickener will be positioned after the oil recovery unit and prior to the anaerobic digesters so as firstly to prevent the solid particles from floating as they are dragged by the oil moving to the surface, secondly to circumvent the redundancy of the oil recovery unit and lastly to avoid unnecessary modification to the mill layout. This adaptation of the process will not only improve the treatment quality of POME but will prevent heat loss that can be essential to boost the hydrolysis step in anaerobic digestion (Carrere et al. 2016).

To be able to design the thickener unit for an efficient POME treatment, operational parameters such as the flow rate, pressure and the rotational speed of the specific equipment are not sufficient. Data on the material properties of the suspension being dewatered must be readily available across the full range of solids fraction being investigated in the process. The dewatering behavior of the thickener is typically described by the compressional rheology in which the equilibrium extent and rate of separation are determined by the suspension's compressibility and permeability respectively; consequently, these parameters can be quantified by evaluating the so called compressive yield stress, hindered settling function and diffusivity function of the material (Stickland et al., 2005; Usher & Scales, 2005). However, the rheological characteristics and compressive behavior of POME have scarcely been studied, so much so that POME has not been physically characterized. This paper attempts to bridge the gap on the study of the physical properties of POME by determining the compressive yield stress; the hindered settling function, the diffusivity function as well as some relevant solids content represented by the solids volume fractions. These are firstly the initial solids volume fraction, ϕ_0 present in the suspension, the gel point, ϕ_g and the closed packed solids volume fraction, ϕ_{cp} (Usher & Scales, 2005; Usher et al., 2009; Zhang et al., 2015). These parameters will provide a broader understanding of the dewatering properties and the compressive behavior of POME as well as fundamental specifications required for the design of the thickener device.

The rest of this work is laid out as follows; Section 2 relates the background on the different rheological parameters relevant to this study. Section 3 describes the material used and the experimental procedures undertaken in this study and Section 4 presents and examines the results obtained. Finally, Section 5 gives the conclusions on this study.

2 Background

2.1. Compressive Yield Stress, $P_y(\phi)$.

Suspension compressibility is dependent upon the extent of dewatering and can be characterized by the compressive yield stress, $P_y(\phi)$. $P_y(\phi)$ dictates the solids volume fraction, ϕ, to which a suspension will be dewatered at an applied pressure, ΔP. Particles in most suspensions when left to settle for a significant period of time, form an inter-connected particle network which is capable of supporting its own weight under gravity (Harbour et al., 2001). The solids volume fraction at which the network starts to form is known as the gel point, ϕ_g. Therefore, a suspension will only exhibit a compressive yield stress if the solids concentration is greater than ϕ_g. When an external stress i.e. a pressure, ΔP, is applied to the network, it collapses and irreversible particle consolidation occurs (Aziz et al., 2000; De Kretser et al., 2001; Harbour et al., 2001; Zhang et al., 2015). As the solids volume fraction, ϕ, increases, the number of inter particle bonds increases which consequently causes $P_y(\phi)$ to increase. Dewatering continues until $P_y(\phi)$ is equivalent to the applied pressure, ΔP, at which the system has reached equilibrium.

The functional form of the compressive yield stress $P_y(\phi)$ can be represented by using a compressive yield stress empirical equation (1) formulated by Zhang et al. (2015b)

$$P_y(\phi) = \frac{C_0\left(\phi - \phi_g\right)^{k_o}}{(b_0 + \phi - \phi_g)^{k_0} * \left(\phi_{cp} - \phi\right)^{k_0}} \qquad (1)$$

Where; $P_y(\phi)$ is the compressive yield stress measured in Pa, ϕ_g is the gel point, ϕ_{cp} is the close packing solids volume fraction. Specifically, ϕ_{cp} is the close packing solids fraction which can never be surpassed as the compressive yield stress tends towards infinity, $P_y(\phi) \rightarrow \infty$ (Zhang et al., 2015b). Moreover, C_0 measured in Pa, b_0 and k_0 which are dimensionless parameters that are dependent on the suspension properties.

2.2 Hindered Settling Function, R(ϕ)

The hindered settling function, R(ϕ) takes into consideration the hydrodynamic interactions between particles or more commonly between flocs of particles grouped together in a consolidating suspension. R(ϕ) is finite at all solids volume fractions and typifies the consolidation rate of the suspension at any given concentration explicitly or in other words, R(ϕ) quantifies the dewatering rate (Green et al., 1998). The permeability, k(ϕ) measured m^2 can be expressed in terms of R(ϕ). From equation (2), it is seen that the permeability of a material is inversely proportional to the hindered settling function, R(ϕ) (Usher et al., 2001):

$$k(\phi) = \frac{\eta}{R(\phi)} \frac{(1-\phi)}{\phi} \tag{2}$$

Where; η is liquid viscosity, $R(\phi)$ is the hindered settling function and ϕ is the solids volume fraction.

Unlike compressive yield stress which is identically zero below the gel point, ϕ_g , the hindered settling function below the ϕ_g can be evaluated in the low solids volume fraction regime through batch settling experiments provided the initial solids volume fraction, ϕ_0, of a suspension is known (Lester et al., 2005). Using the data from the batch settling experiment, the settling velocity can be evaluated through the slope of the interfacial height versus time graph. The analyses of Grassia et al., (2008); Lester et al., (2005) stated that the settling flux, f(ϕ), the settling velocity, u(ϕ), and the solids volume fraction, ϕ, are related via the equation (3)

$$f(\phi) = \phi\, u(\phi) \tag{3}$$

Lester et al. (2005) gave equation (4) to calculate R(ϕ) from the batch settling experiments based on the settling flux, f(ϕ)

$$R(\phi) = -\left(\frac{(1-\phi)^2}{f(\phi)}\right)\Delta\rho g\phi \quad (4)$$

Where; f(ϕ) is the settling flux in m/s, R(ϕ) is the hindered settling function in Pa s/m^2, $\Delta\rho$ is the difference in solid-liquid densities, g is acceleration due to gravity (9.81m/s^2) and ϕ is the solids volume fraction. Since the settling velocities and the settling fluxes are downwards in direction, the minus sign is introduced to ensure that R(ϕ) remains positive.

To determine R(ϕ) above ϕ_g, de Kretser *et al.* (2001) designed a rapid filtration measurement technique to determine dewatering parameters i.e. R(ϕ) and another parameter to be defined shortly D(ϕ). De Kretser *et al.* (2001) indicated that during the cake formation stage of filtration, the correlation between time, t and the specific volume of filtrate, V (where the volume is expressed per unit area of membrane), followed a quadratic relationship such that the plot of t versus V^2 produced a linear correlation. The inverse of the slope of this linear portion is denoted by β^2. They also investigated how the slope of the plot β^2 versus ΔP can be used to calculated R(ϕ) above ϕ_g as shown in equation (5)(Usher *et al*,. 2001).

$$R(\phi_\infty) = \frac{2}{\frac{d\beta^2}{d\Delta P}}\left(\frac{1}{\phi_0} - \frac{1}{\phi_\infty}\right)(1-\phi_\infty)^2 \quad (5)$$

Where; ϕ_0 is the initial solids volume fraction, ϕ_∞ is the equilibrium solids volume fraction at the corresponding applied pressure. Using equations (4) and (5), it is possible to determine the values of R(ϕ) over the full range of solids volume fractions.

2.3 Diffusivity Function, D(ϕ)

The solids diffusion coefficient also known as the diffusivity function, D(ϕ) designates the interaction between the hindered settling behavior, the compressibility and the solids content of a suspension (Landman et al., 1999; Scales, 2006). D(ϕ) represents a parameter which can fully characterize the dewaterability of a suspension. D(ϕ) characterizes the dewatering process by combining both the extent of filtration i.e. $P_y(\phi)$ (which expresses the compressibility of

the suspension) and the rate of filtration, related inversely with R(ϕ) (which expresses the permeability of the suspension) as presented in equation (6) (Stickland et al., 2008; Raha et al., 2005; Usher et al., 2001):

$$D(\phi) = \frac{(1-\phi)^2 \frac{dP_y(\phi)}{d\phi}}{R(\phi)} \quad (6)$$

Where; is $\frac{dP_y(\phi)}{d\phi}$ the differential of the compressive yield stress, ϕ is the solids volume fraction and $R(\phi)$ is the hindered settling function. It has been proven mathematically that D(ϕ) is inversely proportional to the time taken for a suspension to dewater (Harbour et al., 2001; Scales, 2006). As such a simple comparison of dewaterability can be established by comparing D(ϕ) on an equal solids volume fraction scale. The proper interpretation of the information of the D(ϕ) versus the solids volume fraction plot conveys is essential; it is found that a plot shifted more towards the right towards higher solids volume fraction tends to be more compressible and a plot shifted upwards shows a higher diffusivity function indicating a shorter filtration time (Harbour et al., 2001; Skinner et al., 2015).

Moreover, a convenient and consistent way to calculate the diffusivity function via pressure filtration data is by using equation (7) presented by de Kretser *et al.* (2001).

$$D(\phi_\infty) = \frac{1}{2}\frac{d\beta^2}{d\phi_\infty}\left(\frac{1}{\phi_0} - \frac{1}{\phi_\infty}\right)^{-1} \quad (7)$$

Where; ϕ_0 is the initial solids volume fraction, ϕ_∞ is the equilibrium solids volume fraction at the corresponding applied pressure.

To summarize, the discussion above has illustrated what the key parameters characterizing the dewatering of a suspension are. The next sections focus specifically upon how these are to be obtained in the case of POME.

3 Materials and Methods

3.1 Materials

Hot POME (65^{o}C) was obtained at the Seri Ulu Langat Palm Oil Mill, Dengkil, Malaysia. The sample site lies within longitude 03^{0}, 11', and 52.5" N and latitude 101^{0}, 18' and 23.7" E. The temperature of POME at the collection location was measured to be 65°C. The temperature drop from the discharged temperature (80-90°C) can be attributed to the heat loss through the pipeline as it reaches the sampling location. In order to mimic industrial conditions, the hot POME samples were stored at 65°C using a thermos flask and used within 12 hours upon collection. Otherwise, the samples were kept refrigerated at 4°C until further use.

3.2 Methods

3.2.1. Physico-chemical properties

The physico-chemical properties experiments for POME such as the Chemical Oxygen Demand (COD), Biochemical Oxygen Demand (BOD), Total Solids (TS), Total Suspended Solids (TSS), volatile solid (VS), and oil and grease were conducted as per the Standard Methods approved by the United States Environmental Protection Agency (US EPA) which is in accordance to ASTM standards (ASTM 2000). Table 1 lists the physico-chemical compositions of the POME:

Table 1: Physico-chemical properties of POME

Parameters	Raw
Solids volume fraction / v/v	0.177±0.003
COD/ mg/L	44800±3500
BOD/ mg/L	21950±1000
TS/ mg/L	48680±3400
VS/ mg/L	993±60

Oil and grease/ mg/L	653±0.3
Temperature/ °C	65±2.8
pH	4.64±0.3

3.2.1 Batch Settling Experiment

The batch settling experiments were undertaken at a constant temperature of 65°C to mimic industrial conditions but for different dilutions of POME. POME was diluted with distilled water to cater for different solids fractions. The concentrations considered were raw, 2, 4, 6 and 8 times diluted POME. Different dilutions of POME were then transferred into 5 identical 100mL measuring cylinders which were in turned placed in a water bath at 65°C. The height of the interface, h, between suspension and liquor was measured with time for each sample. The experiment ended when the interfacial height remained constant for a period of 3 hours. The experiments were undertaken at different dilutions of POME to allow the evaluation of the hindered settling function, $R(\phi)$ below the gel point, ϕ_g. The experiments were repeated with cold POME thawed to room temperature (CPTRT) at 28°C and cold POME which was allowed to settle in a thermostatic cabinet at 10°C to investigate the effect of temperature on the settling properties of POME. The media in all the experiments were unstirred to allow settling by gravity. Figure 1 shows the experimental set up for the batch settling experiments. From the batch settling experiments, data such as the settling velocities $u(\phi)$, the settling fluxes, $f(\phi)$ and the hindered settling function, $R(\phi)$ below the gel point, ϕ_g, were obtained.

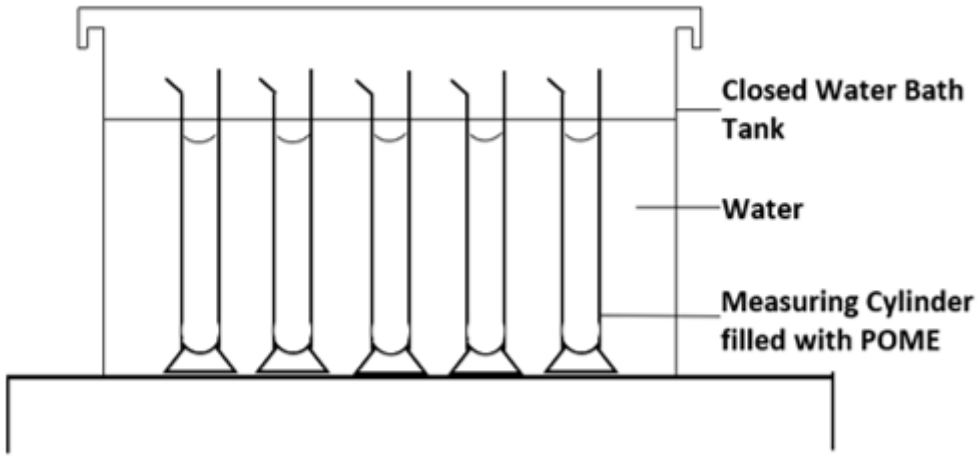

Figure 1: Batch Settling Experimental Set Up

Figure 2 depicts the schematic illustration for the consolidation of a suspension where h_0 is the initial interfacial height and $Z_c(t)$ is the position at which the consolidation region meets free-falling flocs, implying a rapid transition from free falling individual flocs at $\phi = \phi_0$ to $\phi = \phi_g$.

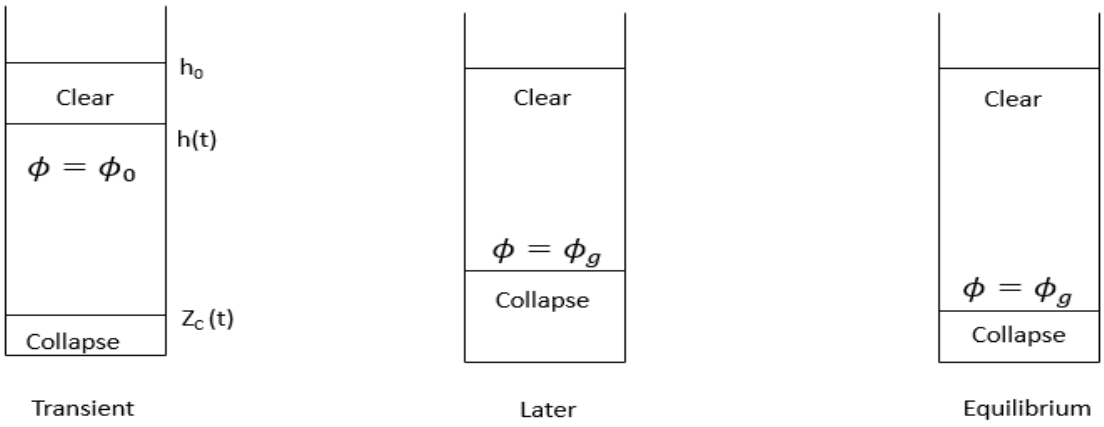

Figure 2: Schematic illustration of consolidating suspension when $\phi_0 < \phi_g$

In this study, solely the initial rate of change of h was measured. However, it was noted that rates of change of h at later stages can furnish additional rheological information (Lester et al., 2005).

3.2.2 Batch Filtration Experiment

A single pressure filtration technique was employed for the batch filtration experiment. This method involves the application of a single constant pressure which enables the determination of a single compressibility and permeability value for each test. Single pressure filtration is a suitable filtration technique for measuring suspension rheological properties; however, it requires a significant amount of time with five or more individual filtration tests required to characterize a sample effectively (Usher et al., 2001). Stepped pressure filtration can potentially cut down the experiment time (de Kretser et al. 2001) but in this study, the latter was not utilized. The batch filtration experiment was undertaken in a stirred pressure cell (Brand: Sterlitech HP 4750). The stirrer was set at 150rpm. POME samples for hot POME, CPTRT, and cold POME were filtered at constant gauge pressures ranging from 100 -500kPa. Pressure was applied by air filtration rather than with the use of a piston and the system was tightly sealed with a membrane separating the blown air from the suspension to prevent desaturation. 50 mL of the sample was placed into the stirred pressure cell, the required pressure was set, and the experiment was allowed to run. In order to monitor the evaporation taking place during the filtration experiment, a beaker of 50mL of water at 65°C, 28°C and 10°C for hot, CPTRT and cold POME respectively were placed under the same conditions as the filtrate. The initial mass was measured using an electronic balance (Brand: A&D scales model FX-3000i) which sent the recorded data directly to a software and volume of water were recorded. Once the filtrate mass remained constant for up to an hour, the experiment was stopped. The final mass and volume of water along with that of the filtrate were measured. Figure 3 shows the experimental set up for the batch filtration experiments. The experiments were repeated with cold POME and CPTRT to investigate the effect of temperature on the rheological characteristic of POME.

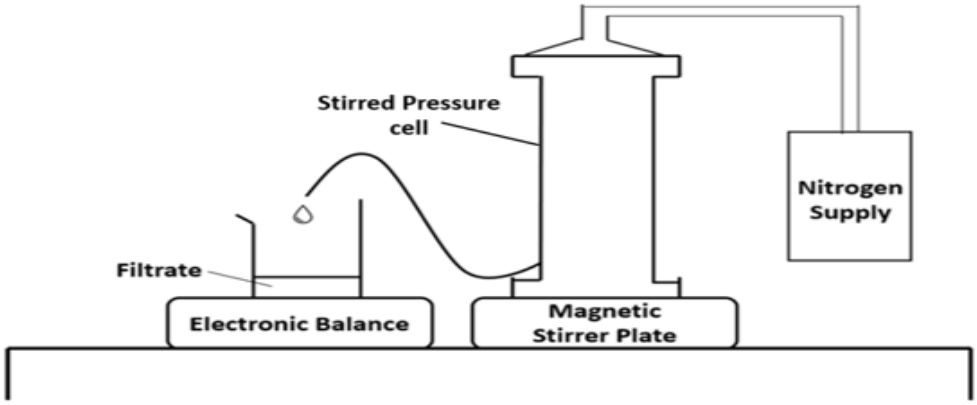

Figure 3: Batch Filtration Experimental Set Up

A significant challenge was finding the initial solids volume fraction in the sample of POME used since the composition and chemical characteristics of POME vary from batch to batch when sampled. The method for evaluating the initial solids volume fraction is discussed below.

3.3 Initial solids volume fraction, ϕ_0

For the determination of the initial solids volume fraction, ϕ_0, 3 different batches of POME sample were used to undertake pressure filtration experiments and were ran at a pressure of 100kPa. Once the filtrate volume was constant for up to an hour, the cake obtained at the end of the experiment was oven dried at 105°C and weighed until the weight remained constant (Stickland, 2015). The equations below were used to determine the initial solids volume fraction, ϕ_0. The mass balance for the filtration system is as shown below:

$$M_T = M_{TC} + M_{FF} \quad (8)$$

Where M_T is the mass of suspension, M_{TC} is the mass of the cake after filtration (which consists of the mass of solid and liquid in the cake) and M_{FF} is the mass of the final filtrate. The above equation should be rewritten in terms of volume since in this study the solids volume fraction is the parameter of interest (Landman & White, 1994; Perlmutter & White, 1994).

$$V_{TC} = V_T - V_{FF} \quad (9)$$

Where V_T is the volume of suspension, V_{TC} is the volume of the cake after filtration and V_{FF} is the final filtrate volume. The cake consists of mostly solid flocs and entrapped liquid. To be able to determine the volume of solids present in the cake, the cake was oven dried to remove the liquid present and was weighed. Equation (10) expresses V_{TC} in terms of masses and densities of the solid and liquid found in the cake.

$$V_{TC} = V_{SC} + V_{LC} = \frac{M_{SC}}{\rho_s} + \frac{M_{LC}}{\rho_l} \quad (10)$$

Where V_{SC} is the volume of solids in the cake, V_{LC} is the volume of liquid in the cake, M_{SC} is the mass of solids in the cake, M_{LC} is the mass of liquid in the cake, ρ_s is the density of the solids and ρ_l is the density of the filtrate. From the filtration experiments, V_{FF}, M_{FF}, V_{TC} and ρ_l can be known. After drying the cake, M_{SC} can be measured and assuming the solids are present as suspended solids rather than dissolved solids hence M_{LC} and V_{LC} can be calculated. It is therefore possible to compute ρ_s to be able to evaluate V_{SC} by subtracting V_{LC} to V_{TC}. Once the value for V_{SC} is evaluated. The initial solids volume fraction can therefore be determined using equations (11- 13)

$$V_{SC} = \phi_0 * V_T \quad (11)$$

$$V_{SC} = \phi_\infty * V_{TC} \quad (12)$$

$$V_{SC} = \phi_0 * V_T = \phi_\infty * V_{TC} \quad (13)$$

Where ϕ_∞ is the solids volume fraction at equilibrium in the cake after filtration which can also be expressed as V_{SC}/V_{TC}. Equation 13 demonstrates that the total volume of solids in the suspension equals to the total volume of solids in the cake as no solids pass through to the filtrate as the solids are assumed to be suspended rather than dissolved. To ensure that the assumption was valid, the filtrate was dried off and the dissolved solids volume fraction was calculated. The dissolved solids volume fraction in the filtrate was evaluated to be

0.0186±0.0027 v/v; as this value is significantly less than 1, it is valid to assume that the dissolved solids in this study is negligible. Combining equations 9 and 13 and the values of V_{SC}, V_{TC}, V_T and V_{FF}, ϕ_0 was found as shown in equation 14.

$$\frac{V_{SC}}{V_{TC}} = \frac{\phi_0 * V_T}{V_T - V_{FF}} \quad (14)$$

The initial solids volume fraction found for the 3 batches were 0.177, 0.183 and 0.171. Therefore, the initial solids volume fraction used for the study was 0.177±0.003. Hence equation (15) was used to determine ϕ_∞ after each filtration experiment

$$\phi_\infty = \frac{0.177 * V_T}{V_{TC}} \quad (15)$$

Where V_T and V_{TC} are dependent on the pressure and temperature of each filtration experiment. The liquid density at 10, 28 and 65°C were found to be around 1000.4, 1000.2 and 999.9 kg/m3 respectively. It was observed that within the studied temperature range the variation in the liquid densities were negligible compared to the difference between the solid and liquid density. Therefore, the liquid density used for the calculations was 1000 kg/m^3. From the above analysis, the solid density within the suspension was evaluated to be 1100 kg/m^3. It is worth noting however that the relatively low density difference between solids and liquid may limit the extent to which a gravity thickener may dewater a POME suspension. These densities values will further aid in the calculation of the hindered settling function, R(ϕ) below the gel point, ϕ_g.

4 Results and Discussion

4.1 Batch Settling

The batch settling experiments of 2, 4, 6 and 8 times dilutions of POME accounting for solid volume fractions of 0.089±0.004, 0.0443±0.001, 0.030±0.002 and 0.022±0.001 v/v

respectively were undertaken to assist in the evaluation of the gel points of POME as well as to examine the behavior of R(ϕ) below the gel point. Figure 4 shows the batch settling results for Hot POME at a constant temperature of 65℃.

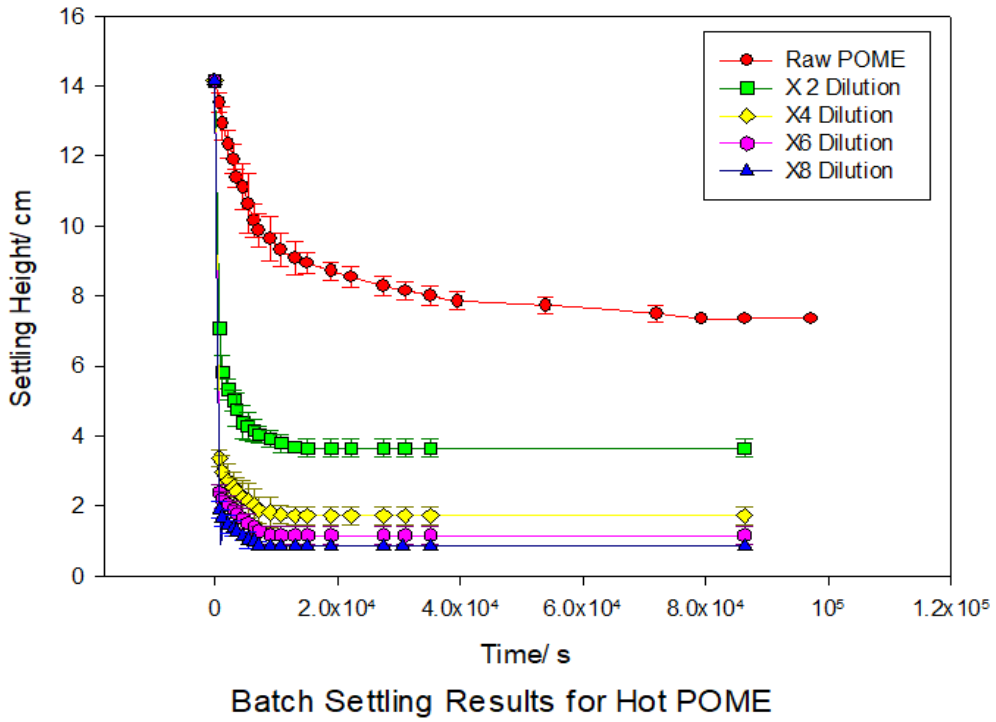

Figure 4: Batch Settling results for Hot POME

It can be observed that the settling rate for raw POME is considerably lower than 2,4, 6 and 8 times dilutions. The final bed heights for raw, 2, 4, 6 and 8 times dilutions were 7.3, 3.6, 1.7, 1.1 and 0.8 cm respectively for a 14.1 cm initial height. Figure 4 shows data for Hot POME, batch settling tests were also conducted for diluted CPTRT and Cold POME. However, there was a constraint to the batch settling experiments of CPTRT and Cold raw POME. Raw POME does not settle at room temperature and below, instead the solid particles present in the suspension tend to rise to the surface or form distinct lumps of solid particles floating with the liquid medium along the settling column. Some possible explanations for the latter behavior are firstly, POME starts to decompose at these temperatures producing biogas that causes distinct mass of particles to float as the biogas rises; while for Hot POME, the microorganisms

409 responsible for the decomposition of POME cannot thrive at such a high temperature, therefore
410 no biogas is produced, and the flocs settle normally. Secondly, the initial solids volume fraction
411 may be greater than the gel point however owing to being a weak networked suspension at
412 these temperatures the flocs in the suspension do not settle.

413 ## 4.2 Compressive Yield Stress, $P_y(\phi)$
414

415 As mentioned earlier, batch filtration was used as the primary means of determining $P_y(\phi)$.
416 As the filtration experiment reaches the end, the filtrate volume remains constant, no more
417 consolidation occurs, and the filter cake has a uniform solids concentration at the equilibrium
418 solids volume fraction,ϕ_∞. At equilibrium, the sample has stopped compressing for a given
419 applied pressure i.e., the compressive yield stress $P_y(\phi_\infty)$, at the equilibrium solids volume
420 fraction can be thus equated to the applied pressure (de Kretser et al., 2001; Green et al., 1996;
421 Landman et al., 1995). Zhang *et al.* (2015b) states that the compressive yield stress can exhibit
422 different types of variation in the neighborhood of the gel point, ϕ_g. Zhang *et al.* (2015a)
423 suggested an empirical equation to fit the compressive yield stress $P_y(\phi)$ as shown in equation
424 1. However, in the present study equation (1) was rewritten in such a form that the constants
425 C_0, b_0 and k_0 were collapsed together into a single parameter denoted by X_0 ($X_0 \equiv C_0/{b_0}^{k_0}$),
426 since compared to Zhang *et al.* (2015b) study, in the case assuming $\phi - \phi_g \ll b_0$ some
427 parameters are redundant (Stickland, 2015; Zhang et al., 2015a). The form in which equation
428 1 reduces in the neighborhood of the gel point is shown below.

429 $$P_y(\phi) = X_0 * \left(\frac{\phi - \phi_g}{\phi_{cp} - \phi}\right)^{k_0} \quad (16)$$

430 Using the data obtained from the pressure filtration test and equation (16), X_0, ϕ_g, ϕ_{cp} and k_0
431 were estimated by data fitting. Table 2 presents the values obtained for X_0, ϕ_g, ϕ_{cp} and k_0 for
432 hot, CPTRT and cold POME.

Table 2: Compressive yield stress fitted parameters

POME sample	$X_0 \equiv C_0/{b_0}^{k_0}$/ Pa	ϕ_g/ (v/v)	ϕ_{cp}/ (v/v)	k_0
Hot (65°C)	2.132±0.094	0.380±0.030	0.980±0.025	1.372±0.030
CPTRT (28°C)	1.968±0.095	0.352±0.050	0.970±0.010	1.364±0.003
Cold (10°C)	1.950±0.040	0.321±0.047	0.961±0.010	1.356±0.009

From Table 2, it can be established that X_0 and ϕ_g are temperature sensitive parameters while ϕ_{cp} and k_0 proved to be unresponsive to temperature change. The fitted gel point decreased with decreasing temperature, as did X_0. An explanation for X_0 to show changes with temperature is due to the compensation for the temperature dependence of ϕ_g. As for the high ϕ_{cp} values (predicted very close to unity), this occurrence can be due to the residual or bound water in the nominally solid particles or tentatively due to the dissolved solids in the liquid phase which has been neglected here. The data shown above is unique in the study of the rheology of POME since no previous research has been undertaken on this aspect of POME and no such findings have formerly been presented. It can thus be concluded based on these filtration data that the initial solids volume fraction, ($\phi_0 = 0.177$) lies below the gel point, ϕ_g as the ϕ_g of hot, CPTRT and cold POME which were evaluated to be 0.380±0.030 v/v, 0.352±0.050 v/v and 0.321±0.047 v/v respectively. When designing a thickener, it is essential to know whether the feed suspension is networked ($\phi_0 > \phi_g$) or unnetworked ($\phi_0 < \phi_g$) as this will consequently dictate the design and operation of the dewatering device. Landman & White (1994) stated that knowing whether the feed is networked or not is fundamental as the operator may have less straightforward control on the flux if the feed input is unnetworked. The unnetworked mode can still however be used to its advantage as such a system can be used to clarify the suspension, albeit the underflow will be networked. Additionally, a benefit of an unnetworked suspension is that the latter can be flocculated by the addition of appropriate

polymers to enhance the settling rate (Deniz 2015). The latter is a potential advantage for thickening with unnetworked suspension.

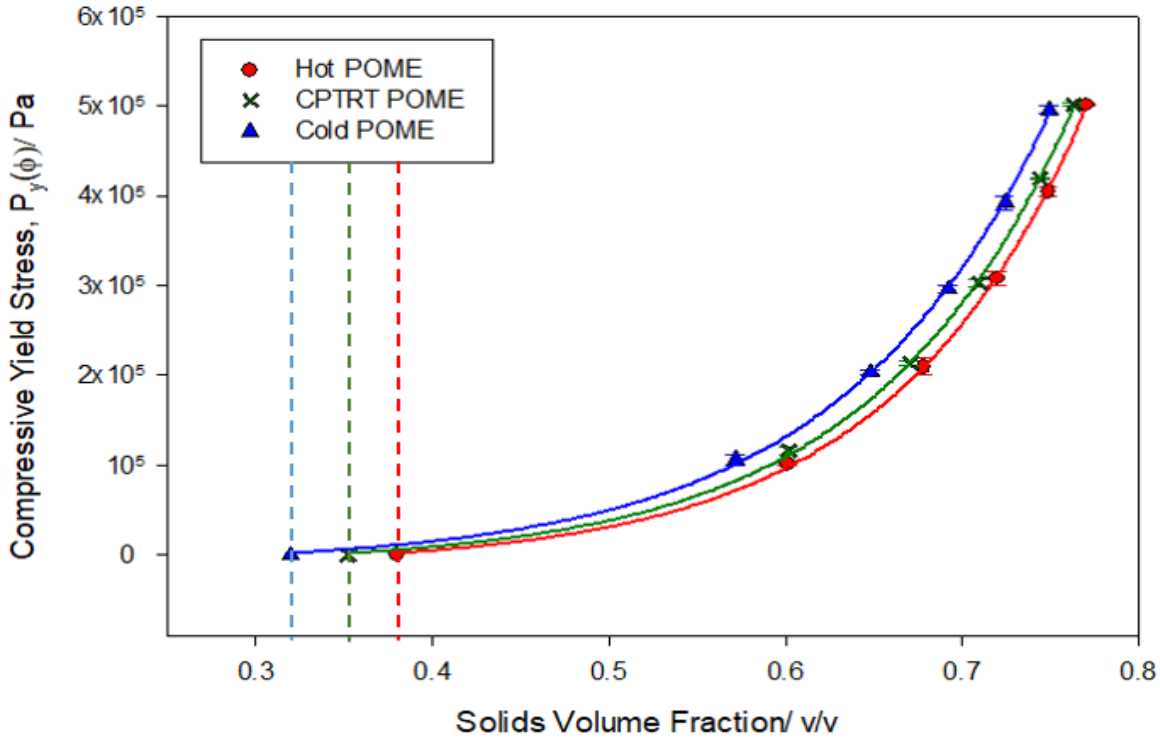

Figure 5: Graph of compressive yield stress, $P_y(\phi)$ for hot, CPTRT and Cold POME versus solids volume fraction

Fitted P_y versus ϕ curves were plotted in Figure 5. The dash lines in Figure 5 represents the gel points, ϕ_g of POME at the different temperatures; 65°C for hot, 28°C for CPTRT, and 10°C for cold POME. Figure 5 shows that hot and CPTRT POME have higher gel points, ϕ_g than Cold POME. According to Table 2, the close packing volume fractions, ϕ_{cp}, are also slightly higher compared to cold POME although the value of ϕ_{cp} is still some way away from the range of ϕ plotted in the above figure. This implies that hot and CPTRT POME are more compressible than cold POME as the graphs for hot and CPTRT POME lie more towards the right. The trends of the compressive yield stress graphs for hot and CPTRT POME are found to be very close to each other. When comparing the compressive yield stress graphs of hot and

CPTRT POME, it can be noted that the data points on the hot POME graph lie more to the right compared to that of CPTRT, this shows that hot POME is slightly more compressible that CPTRT and subsequently has a lower compressive yield stress. The coefficients of correlation squared, R^2, can be used to validate a prediction in this case $P_y(\phi)$ based on experimental data; the higher the value of R^2, the more effective is the validation. The values of R^2 for hot, CPTRT and cold POME correlations of $P_y(\phi)$ were found to be 0.9996, 0.9993 and 0.9989 respectively, indicating that the correlations for $P_y(\phi)$ for hot, CPTRT and cold POME were good fits over the ϕ range taken into consideration. This however does not mean that the fits are necessarily good extrapolating outside the range of ϕ studied. Batch pressure filtration data in general tend to correspond to ϕ values above the gel point, so the gel point here has been estimated via extrapolation and the estimate might not be accurate as a consequence. Another minor issue is the distinction between equations (1) and (16). In fact, (16) to which the curves were fitted is a specific case to (1) assuming that $\phi - \phi_g \ll b_0$. However, if $\phi - \phi_g \gg b_0$, the (1) approximate to $C_0(\phi_{cp} - \phi)^{k_0}$. This no longer involves the gel point, ϕ_g as a parameter making it no longer possible to estimate ϕ_g from the curve fit to data restricted to the domain $\phi - \phi_g \gg b_0$.

Batch settling experiments tend to be more appropriate than batch filtration when it comes to the investigation of the behavior of a suspension close to the gel point.

Figure 6 shows the variation of time, t/s versus specific volume of filtrate squared V^2/m^2 recorded for a typical POME filtration experiment. The figure further illustrates that POME behaves traditionally and is characterized by long cake formation times (up to 85% of the total filtration time) followed by short compression times (Harbour & Scales, 2002; Stickland et al., 2008; Stickland et al., 2005); this observation is in concurrence with Stickland *et al*. (2005)

study. However, an abnormal jump was observed in all the POME filtration t/s versus specific volume of filtrate squared V^2/m^2 graphs.

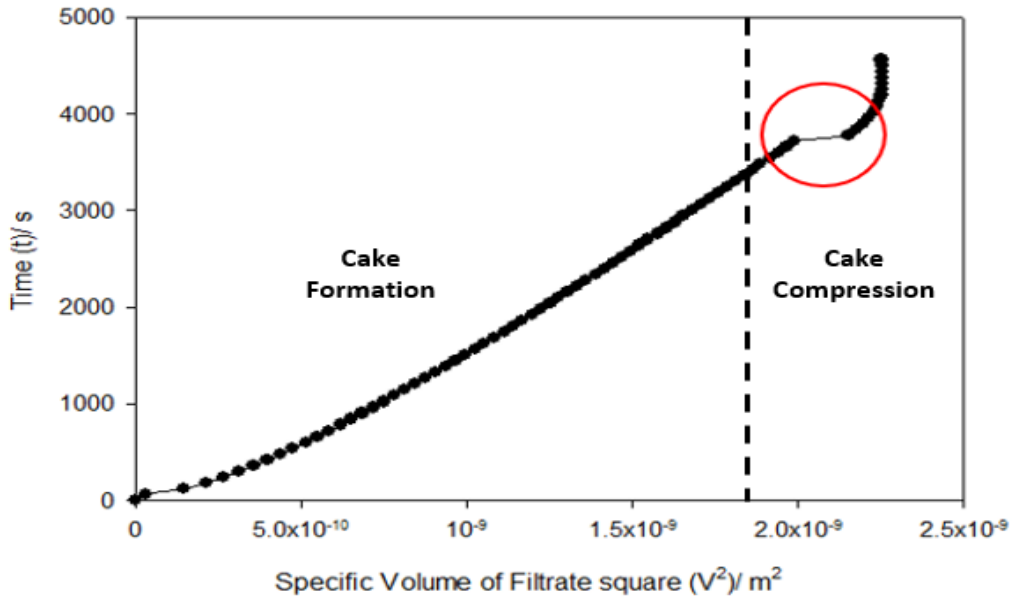

Figure 6: Graph of time, t versus specific volume of filtrate square, V^2

The atypical jump in Figure 6 could be explained under the condition that the initial solids volume fraction, ϕ_0 lies below the gel point, ϕ_g. De Kretser *et al.* (2001) identified a similar occurrence when using a suspension with lower solids volume fraction than the latter's gel point, ϕ_g; this anomaly is directly attributed to sedimentation of the suspension within the filtration cylinder during the time frame of the experiment, leaving some clear liquid adjacent to the cylinder that is expelled later on once the cake is formed (De Kretser et al., 2001). Sedimentation occurs early on since there is no solids network stress gradient to support the particles at this particular stage of the experiment, therefore, the individual flocs are in free fall at the top of the filtration cylinder, as illustrated in Figure 2, albeit hindered by the hydrodynamics interaction with neighboring flocs.

4.3 Hindered Settling Function, R(ϕ)

The hindered settling functions, R(ϕ) below the gel point, ϕ_g, were calculated based on the batch settling experiment results. Once the settling flux, f(ϕ) was found, the value was substituted in equation (4) to find R(ϕ) below the gel point, ϕ_g. As for the determination of R(ϕ) above the gel point, ϕ_g, the slopes resulting from the graphs of t versus V^2 at different pressures obtained from the filtration experiment were calculated i.e. the values, of β^2. A graph of β^2 versus the applied pressure was plotted to find $\frac{d\beta^2}{d\Delta P}$. The value for $\frac{d\beta^2}{d\Delta P}$ was substituted in equation (5) based on de Kretser *et al.* (2001) study. The graphs of the hindered settling functions in log scale were plotted versus solids volume fraction, as shown in Figure 7.

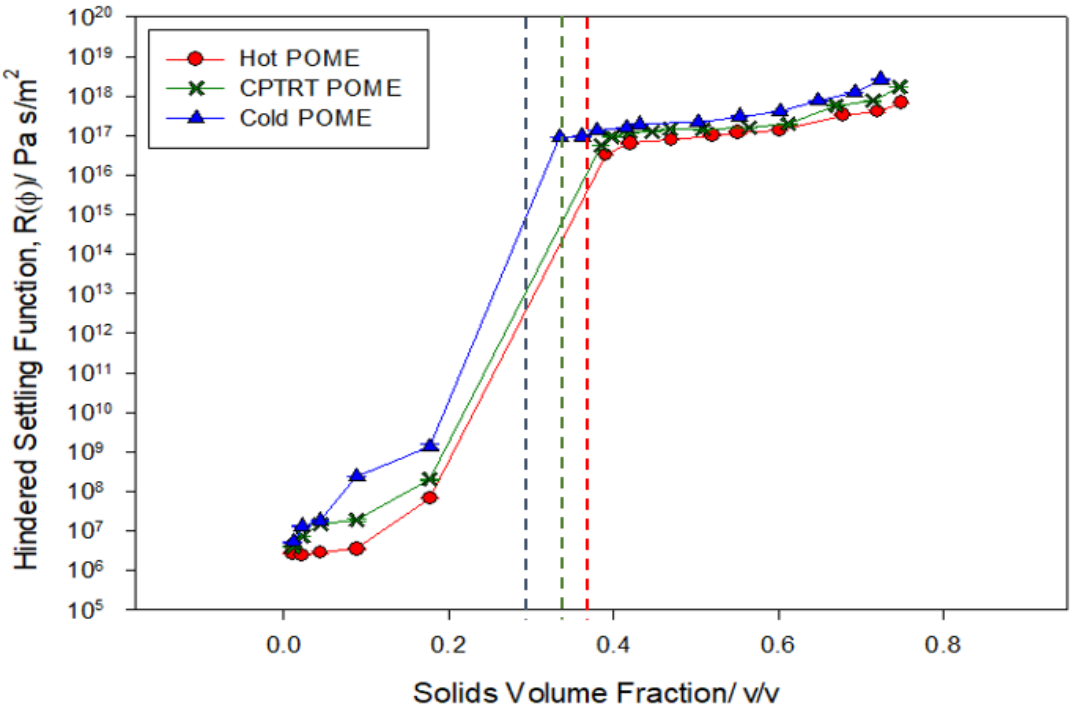

Figure 7: Graph of hindered settling function, R(ϕ) in log scale for hot, CPTRT and Cold POME versus solids volume fraction

Stickland et al. (2008) study on wastewater treatment sludges exhibited R(ϕ) as high as that of POME at higher solid concentrations. Stickland et al. (2008) described wastewater treatment sludge as a weak permeable network at low solids volume fractions but with a very low permeability at high solids volume fractions. It was observed that POME exhibits a similar

behavior to such wastewater treatment sludges; with low R(ϕ) at lower solids volume fraction and high R(ϕ) at higher solids volume fractions which indicates that POME tends to be impermeable at high solids volume fractions. Figure 7 shows the trends for the hindered settling function for hot, CPTRT, and cold POME against different solids volume fractions. The R(ϕ) for hot POME at 0.771v/v was evaluated to be 8.75×10^{17} Pa s/m^2, for CTRT at 0.769 v/v was evaluated to be 2.35×10^{18} Pa s/m^2 and for cold POME at 0.750 v/v was evaluated to be 3.26×10^{18} Pa s/m^2. It is seen in Figure 7 that hot POME has a substantially lower R(ϕ) compared to CPTRT and cold POME. Although batch settling data for low solids volume fraction R(ϕ) and batch filtration data for high solids volume fraction R(ϕ) were effectually evaluated, there is a gap covering several orders of magnitude for R(ϕ) which is unaccounted for. Similar results have been observed for wastewater treatment sludges and waste activated sludge (Aziz et al., 2000; Harbour et al., 2001; Stickland et al., 2008; Skinner et al., 2015). As aforementioned, permeability is known to be inversely proportional to the hindered settling function, R(ϕ), as shown in equation (2). The lower the hindered settling function, the more permeable the material is. Hence, it can be established that hot POME is more permeable that CPTRT and cold POME. The findings above demonstrate that hot POME will be dewatered more readily compared to CPTRT and cold POME.

4.4 Diffusivity Function, D(ϕ)

The solids diffusivity function, D (ϕ) is an essential parameter which should be investigated and evaluated to comprehend the dewatering behavior of POME (Usher & Scales, 2005; Zhang et al., 2013). The solids diffusivity function gives an overall measure of the dewaterability of a material, in this case POME (Landman et al., 1995; Landman et al., 1999; Stickland et al., 2005). An alternative definition for D(ϕ) involves the rate at which a concentration gradient propagates through the suspension (Skinner et al., 2015). D(ϕ) is governed by both the

compressive yield stress, $P_y(\phi)$ more specifically $dP_y(\phi)/d\phi$ and the hindered settling function, $R(\phi)$ as shown in equation (6) (de Kretser et al., 2001; Landman et al., 1999; Usher et al., 2001). de Kretser *et al.* (2001) study states that $D(\phi)$ can be determined when the values of the quantity β^2 are plotted against ϕ_∞ and substituted in equation 7 as indicated in Section 2.3. Figure 8 below shows the graphs of $D(\phi)$ versus solids volume fraction for hot, CPTRT and cold POME

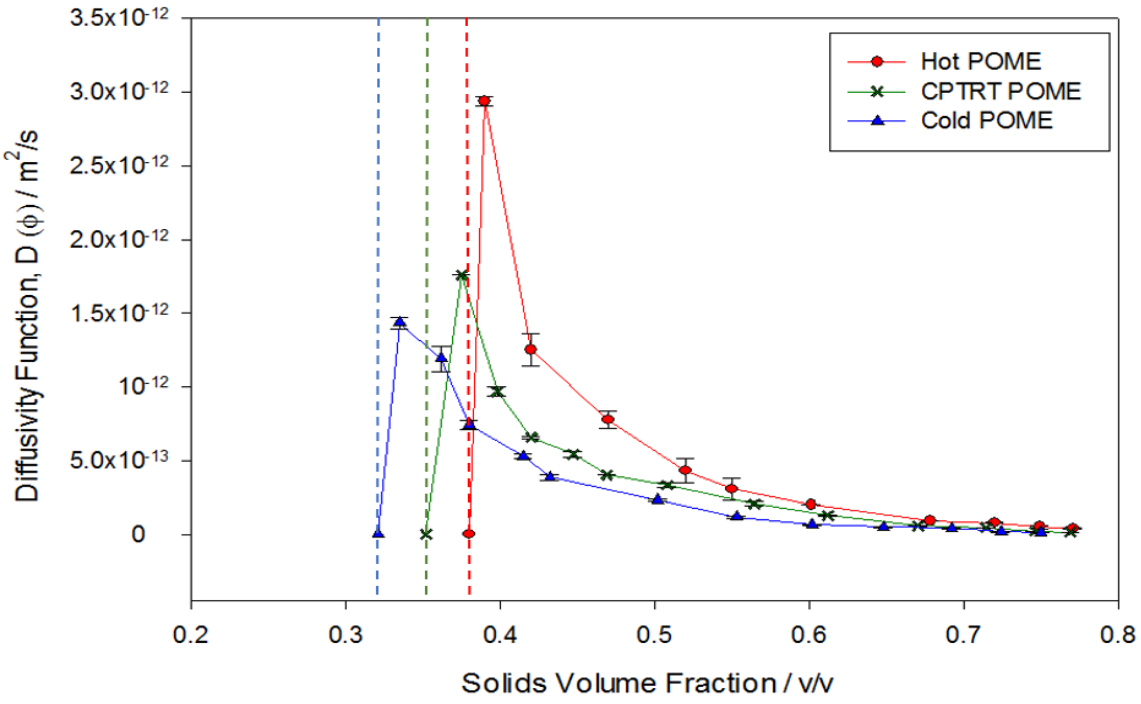

Figure 8: Graph of diffusivity function, $D(\phi)$ for hot, CPTRT and Cold POME versus solids volume fraction

Figure 8 shows that the highest $D(\phi)$ occurs just slightly above the gel point, ϕ_g. By contrast for inorganic suspensions, $D(\phi)$ usually grow monotonically between the initial solids concentration of the feed to the dewatering device and the final solids concentration of the filter cake when equilibrium is achieved (Skinner et al., 2015). However, as observed in Figure 8, this is not the case for POME. There are various explanations for this. Firstly, Skinner *et al.* (2015) described that in nearly every compressible material scenario, $D(\phi)$ peaks nonmonotonically then decreases as the solids volume fraction increases; this trend was

observed when sewage sludge was filtered at high solids concentrations and at high pressures and is in agreement with the rheological study of POME. Secondly, based on equation 5 as ϕ increases, $dP_y/d\phi$ must grow less rapidly than $R(\phi)$. Indeed, from Figure 5, it is observed that the plot $P_y(\phi)$ versus solids volume fraction increases gradually after the gel point while $R(\phi)$ increases sharply as shown in Figure 7. From Figure 8, it can be distinguished that the plot of $D(\phi)$ versus ϕ for hot POME lies well above the plots for CPTRT and cold POME. The highest $D(\phi)$ recorded for hot POME at 0.39 v/v was $2.94x10^{-12}$ m^2/s, for CPTRT POME at 0.385 v/v was $1.76x10^{-12}$ m^2/s, and cold POME at 0.335v/v was $1.43x10^{-12}$ m^2/s. This observation further validates that hot POME will dewater faster than CPTRT and cold POME as a higher $D(\phi)$ designates a shorter filtration time.

It can be concluded that during thickening POME is likely to achieve an underflow solids volume fraction which is just slightly higher than the gel point owing to its low permeability at higher solids volume fractions. To further enhance the dewaterability of POME, the thickening system can be raked so as to bind the individual flocs together more tightly and have correspondingly more liquid in the voids between the flocs (Gladman et al,. 2006; Tan et al,. 2017). With this approach, it is easier for the liquid to be removed through the voids rather than through the flocs themselves. Given that the experiments were repeated, it is worthwhile to note that the extracted hindered settling functions, $R(\phi)$ and the diffusivity function, $D(\phi)$ were reproducible. The latter indicates that the parameter extraction method and the consequent material characterization were well founded for POME.

5 Conclusion

This study has described efforts to quantify the dewaterability of POME alongside a study of the effect of temperature on the rheological properties of POME. From the findings the following conclusions can be established

- Based on the batch filtration data, raw POME was estimated to be an unnetworked suspension as the initial solids volume fractions, ϕ_0, lies below the gel point ϕ_g. This is an interesting finding as this will dictate how the thickener device should be designed and operated.
- Hot POME exhibited a more compressible network compared to CPTRT and cold POME. Since the discharge temperature of POME is already high, it proves to be more advantageous to design a thickener that will be operated using hot POME.
- The hindered settling function for hot POME was substantially lower than CPTRT and cold POME which designates that hot POME is more permeable, as permeability is inversely proportional to the hindered settling function. Subsequently, Hot POME will be dewatered faster owing to its high diffusivity function. Both these dewatering characteristics are favorable for the design of the dewatering device.
- Based on the results obtained, the design of the thickener to improve anaerobic digestion appears feasible as it was established the hot POME is compressible, permeable and can be dewatered relatively fast compared to CPTRT and Cold POME. The dewaterability can be further enhanced by introducing a rake in the thickener for the individual flocs to cohere allowing more liquid in the voids between them.
- A drawback, however, is that the hindered settling function of POME rises rapidly as the solids volume fraction increases, which may limit the solid fraction that a thickener can attain.

Acknowledgment

The authors acknowledge financial support from Monash University Malaysia and the Royal Academy of Engineering under the Newton Research Collaboration Programme (Project NRCP1516/4/34).

References

Anderson, N. J., Dixon, D. R., Harbour, P. J., & Scales, P. J. (2002). Complete characterisation of thermally treated sludges. *Water Science and Technology*, *46*(10), 51–54.

Appels, Lise, Jan Baeyens, Jan Degrève, and Raf Dewil. 2008. "Principles and Potential of the Anaerobic Digestion of Waste-Activated Sludge." *Progress in Energy and Combustion Science* 34 (6): 755–81. https://doi.org/10.1016/j.pecs.2008.06.002.

ASTM. 2000. "American Society for Testing and Materials." Test. 2000. https://www.astm.org/Standards/water-testing-standards.html.

Carrere, Hélène, Georgia Antonopoulou, Rim Affes, Fabiana Passos, Audrey Battimelli, Gerasimos Lyberatos, and Ivet Ferrer. 2016. "Review of Feedstock Pretreatment Strategies for Improved Anaerobic Digestion: From Lab-Scale Research to Full-Scale Application." *Bioresource Technology* 199: 386–97. https://doi.org/10.1016/j.biortech.2015.09.007.

Choong, Y. Y., Chou, K. W., & Norli, I. (2018). Strategies for improving biogas production of palm oil mill effluent (POME) anaerobic digestion: A critical review. *Renewable and Sustainable Energy Reviews*, *82*, 2993–3006. https://doi.org/https://doi.org/10.1016/j.rser.2017.10.036

De Kretser, R. G., Usher, S. P., Scales, P. J., Boger, D. V., & Landman, K. A. (2001). Rapid filtration measurement of dewatering design and optimization parameters. *AIChE Journal*, *47*(8), 1758–1769. https://doi.org/10.1002/aic.690470808

Grassia, P., Usher, S. P., & Scales, P. J. (2008). A simplified parameter extraction technique using batch settling data to estimate suspension material properties in dewatering applications. *Chemical Engineering Science*, *63*(7), 1971–1986. https://doi.org/10.1016/j.ces.2007.12.025

Green, M. D., Eberl, M., & Landman, K. A. (1996). Compressive yield stress of flocculated suspensions: Determination via experiment. *AIChE Journal*, *42*(8), 2308–2318. https://doi.org/10.1002/aic.690420820

Green, M. D., Landman, K. A., de Kretser, R. G., & Boger, D. V. (1998). Pressure Filtration Technique for Complete Characterization of Consolidating Suspensions. *Industrial & Engineering Chemistry Research*, *37*(10), 4152–4156. https://doi.org/10.1021/ie970544i

Harbour, P. J., Aziz, A. A. A, Scales, P. J., & Dixon, D. R. (2001). Prediction of the dewatering of Selected inorganic sludges. *Water Science and Technology*, *44*(10), 191–196.

Hassan, M. A., Yacob, S., Shirai, Y., & Hung, Y. (2005). Treatment of Palm Oil Wastewaters. *Waste Treatment in the Food Processing Industry*, 101–117. https://doi.org/10.1201/9781420037128.ch4

Iskandar, M. J., Baharum, A., Anuar, F. H., & Othaman, R. (2018). Palm oil industry in South East Asia and the effluent treatment technology—A review. *Environmental Technology & Innovation*, *9*, 169–185. https://doi.org/https://doi.org/10.1016/j.eti.2017.11.003

Landman, K. A., Stankovich, J. M., & White, L. R. (1999). Measurement of the filtration diffusivity D(φ) of a flocculated suspension. *AIChE Journal*, *45*(9), 1875–1882. https://doi.org/10.1002/aic.690450905

Landman, K. A., & White, L. R. (1994). Solid/liquid separation of flocculated suspensions. *Advances in Colloid and Interface Science*, *51*, 175–246. https://doi.org/10.1016/0001-8686(94)80036-7

Landman, K. A., White, L. R., & Eberl, M. (1995). Pressure filtration of flocculated suspensions. *AIChE Journal*, *41*(7), 1687–1700. https://doi.org/10.1002/aic.690410709

Lester, D. R., Usher, S. P., & Scales, P. J. (2005). Estimation of the hindered settling function R(φ) from batch-settling tests. *AIChE Journal*, *51*(4), 1158–1168. https://doi.org/10.1002/aic.10333

Perlmutter, B. A. Butterworth-Heinemann, (2015). *Solid-liquid filtration: practical guides in chemical engineering*. Retrieved from http://www.sciencedirect.com.ezproxy.lib.monash.edu.au/science/book/9780128030530

Raha, S., Khilar, K. C., Pradip, & Kapur, P. C. (2005). Rapid determination of compressive yield stress of dense suspensions by a mean-phi ($\bar{\varphi}$) model of high pressure filtration. *Powder Technology*, *155*(1), 42–51. https://doi.org/10.1016/j.powtec.2005.05.040

Scales, P. (2006). *Chapter 13: Dewatering of water treatment plant sludges*. *Interface Science and Technology* (Vol. 10). Elsevier Ltd. https://doi.org/10.1016/S1573-4285(06)80082-7

Skinner, S. J., Studer, L. J., Dixon, D. R., Hillis, P., Rees, C. A., Wall, R. C., Raul, G.C, Usher, S. P, Stickland, A. D, Scales, P. J. (2015). Quantification of wastewater sludge dewatering. *Water Research*, *82*, 2–13. https://doi.org/10.1016/j.watres.2015.04.045

Stickland, A. D., De Kretser, R. G., & Scales, P. J. (2005). Nontraditional constant pressure filtration behavior. *AIChE Journal*, *51*(9), 2481–2488. https://doi.org/10.1002/aic.10501

Stickland, A.D., Burgess, C., Dixon, D. R., Harbour, P. J., Scales, P. J., Studer, L. J., & Usher, S. P. (2008). Fundamental dewatering properties of wastewater treatment sludges from filtration and sedimentation testing. *Chemical Engineering Science*, *63*(21), 5283–5290. https://doi.org/10.1016/j.ces.2008.07.016

Stickland, A. D. (2015). Compressional rheology: A tool for understanding compressibility effects in sludge dewatering. *Water Research*, *82*, 37–46. https://doi.org/10.1016/j.watres.2015.04.004

Tabassum, S., Zhang, Y., & Zhang, Z. (2015). An integrated method for palm oil mill effluent (POME) treatment for achieving zero liquid discharge - A pilot study. *Journal of Cleaner Production*, *95*(May), 148–155. https://doi.org/10.1016/j.jclepro.2015.02.056

Tan, C. K., Bao, J., & Bickert, G. (2017). A study on model predictive control in paste thickeners with rake torque constraint. *Minerals Engineering*, *105*, 52–62. https://doi.org/https://doi.org/10.1016/j.mineng.2017.01.011

Usher, S. P., De Kretser, R. G., & Scales, P. J. (2001). Validation of a new filtration technique for dewaterability characterization. *AIChE Journal*, *47*(7), 1561–1570. https://doi.org/10.1002/aic.690470709

Usher, S. P., & Scales, P. J. (2005). Steady state thickener modelling from the compressive

yield stress and hindered settling function. *Chemical Engineering Journal*, *111*(2–3), 253–261. https://doi.org/10.1016/j.cej.2005.02.015

Usher, S. P., Spehar, R., & Scales, P. J. (2009). Theoretical analysis of aggregate densification: Impact on thickener performance. *Chemical Engineering Journal*, *151*(1–3), 202–208. https://doi.org/10.1016/j.cej.2009.02.027

White, L. R. (1994). Solid- liquid suspensions separation. Solid-liquid separation operations leading to the concentration and isolation of fine particles dispersed in liquids are important in the chemical and mineral processing industries. *51*, 175–246.

Zhang, Y., Grassia, P., Martin, A., Usher, S. P., & Scales, P. J. (2015a). Designing thickeners by matching hindered settling and gelled suspension zones in the presence of aggregate densification. *Chemical Engineering Science*, *134*, 297–307. https://doi.org/10.1016/j.ces.2015.05.016

Zhang, Y., Grassia, P., Martin, A., Usher, S. P., & Scales, P. J. (2015b). Mathematical modelling of batch sedimentation subject to slow aggregate densification. *Chemical Engineering Science*, *128*, 54–63. https://doi.org/10.1016/j.ces.2015.01.066

Zhang, Y., Martin, A., & Grassia, P. (2013). Prediction of thickener performance with aggregate densification. *Chemical Engineering Science*, *101*, 346–358. https://doi.org/10.1016/j.ces.2013.06.055